Proceedings of IDETC/CIE 2005
ASME 2005 International Design Engineering Technical Conferences
& Computers and Information in Engineering Conference
September 24-28, 2005, Long Beach, California USA

DETC2005-85130

CONTROL OF 3D SNAKE-LIKE LOCOMOTIVE MECHANISM BASED ON CONTINUUM MODELING

Hisashi Date
Department of Computer Science
National Defense Academy
Yokosuka, Kanagawa 239-8686, Japan
Email: date@nda.ac.jp

Yoshihiro Takita
Department of Computer Science
National Defense Academy
Yokosuka, Kanagawa 239-8686, Japan
Email: takita@nda.ac.jp

ABSTRACT

An effective control method that achieves movement over a small ridge as an example of three-dimensional (3D) snake-like creeping locomotion is presented. The creeping robot is modeled as a continuum with zero thickness capable of generating bending moment at arbitrary points. Under a simplified contact condition, the optimal bending moment distribution in terms of a quadratic cost function of input can be obtained as a function of curvature by solving an isoperimetric problem. The solution is well suited to an articulated body consisting of finite number of links. The model is demonstrated through simulations and experiments using a prototype robot to be effective for traversing smooth 3D terrain.

Keywords: snake-like robot, continuum modeling, 3D locomotion

1 Introduction

The snake-like locomotive mechanism has long been studied for its capability in moving over complicated and unknown terrain. In recent years, active research has been carried out toward applying this form of locomotion to rescue robots designed to rove through disaster debris. Snakes in nature employ a variety of locomotive gaits in response to the traversing environment, including lateral undulation (serpentine movement), sidewinding, rectilinear locomotion, inchworm, traveling wave, and concertina progression. The features common to all of these gaits are the lack of any limbs and the realization of movement solely by bending their body. Thus, the mechanical structure of the body appears quite simple. However, control is not simple due to the large number of degrees of freedom (DOFs) that need to be controlled properly. The most commonly used gait is lateral undulation, and many species of snake adopt this gait on flat or uneven terrain. The underside of a snake is longitudinally slippery and laterally non-slippery. This form of locomotion is thus achieved by exploiting reaction force from the ground in combination with pushing force to move the body forward using an alternating sideways motion. This form of propulsion results in the well-known S-shape. Similar motion is also employed in other circumstances, such as climbing a tree or swimming underwater. This gait is therefore significant from an engineering point of view. Among the extensive research on this gait, including the analysis and development of prototypes, pioneering research has been conducted by Hirose [1], who proposed the "serpenoid curve". This curve is sinusoidal with respect to an arclength, and its winding approximates a snake's lateral undulation well. The same author also developed an articulated robot with an active cord mechanism (ACM), consisting of 20 rigid links connected in series by rotational joints with a passive wheel to prevent sideslip. Using joint-level servo control, the robot could be made to trace a pre-defined serpenoid curve. This approach was successful for flat terrain, where an arbitrary path can be chosen if no obstacles hinder movement.

Although there have been many such results concerning lateral undulation on flat terrain [2–5], there have been no successes for creeping locomotion on uneven terrain. Several rea-

sons can be conceived for this difficulty. The locomotive mechanism should be capable of three-dimensional (3D) motion in order to adapt to the terrain. Efficient control methods are therefore necessary, as 3D motion is much more complicated than two-dimensional (2D) motion. Furthermore, as no desired path can be drawn a priori given the unpredictability of the rugged terrain, joint-level servoing to a pre-defined trajectory (shape-based control) cannot be applied, requiring some sort of adaptiveness in the controller. It is also hard to model the exact condition of contact between individual modules and an uneven part of the terrain.

In order to overcome these difficulties, a continuum model defined by a continuous backbone curve with zero thickness is introduced to describe 3D motion, and some simplifying assumptions are adopted regarding the contact condition. The idea of a continuum model for control of snake-like mechanisms first appeared in [6–8]. The major advantages of approximating to the continuum model are a reduction in computational cost by describing the kinematics or dynamics according to the curve geometry (i.e., no Jacobian is required), and the good interpretation such an approach offers from a geometric perspective. Chirikjian et al. applied this method to shape-based control using a dynamic model with general form in which the reaction force from the environment was treated as an external force [8]. This formulation cannot be directly applied for creeping locomotion. In the present treatment, the reaction force is incorporated as internal force under a special condition in which the backbone curve never moves in a transversal manner (i.e., perpendicular to the tangent of the backbone curve). By adopting this ambitious assumption, the expression of motion is dramatically simplified compared to the corresponding articulated model with rigid bodies. It is also possible to formulate the problem of the optimal bending moment distribution in terms of a specific cost function as an isoperimetric problem. It turns out that the solution can be expressed as a function of curvature, which is suitable for approximating to the articulated model.

The goal of this paper is to provide an effective control strategy for 3D creeping locomotion according to the optimal solution of the continuum model. In Section 2, a theoretical discussion of the continuum modeling is presented, and the optimal solution is obtained. In Section 3, the experimental system developed for verification is described, and in Section 4, the control strategy for creeping locomotion on a smooth 3D surface is proposed and verified through simulations and experiments.

2 Continuum Model

The continuum model considered is shown in Fig. 1. The body consists of a continuous curve of length L and zero thickness. This curve is called the backbone curve, and is parameterized by the arclength $s \in [0, L]$. A point on the curve at time t is specified by $\mathbf{O}(s,t)$. The derivative with respect to t is marked by an overdot, and the derivative with respect to s is denoted by a prime. In the context of geometry, t is often omitted (e.g., $\mathbf{O}(s)$), even if it is a function of t. $\mathbf{O}(0)$ and $\mathbf{O}(L)$ denote the head and tail, respectively. If not specified, vector values (bold face), their derivatives, and angular velocities are observed from the reference frame fixed to the terrain. From a geometric perspective, the following assumptions are imposed:

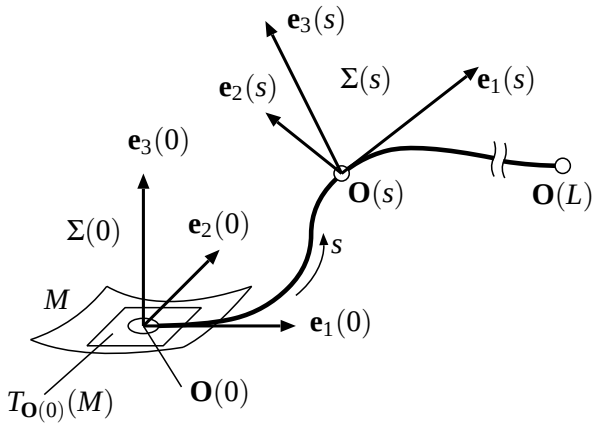

Figure 1. Frame set defined along the backbone curve

Assumption 1.

1. *The terrain surface is a smooth manifold M*
2. *The backbone curve draws a smooth trajectory on the terrain surface*
3. *The body is not stretchable*
4. *The body is torsion-free along the backbone curve*

The first and second assumptions are made for simplicity of manipulating geometric quantities, while the third and fourth are set from the viewpoint of reducing the total DOFs. From assumption 1, at every point $\mathbf{O}(s)$ $(s \in [0, L])$, a reference frame $\Sigma(s)$ is attached to the backbone curve in the following manner. Note that $\Sigma(s)$ is different from the Frenet frame since it is necessary to consider rotation around the backbone curve.

1. The origin of $\Sigma(s)$ is located at $\mathbf{O}(s)$
2. The orthonormal bases $\mathbf{e}_1(s)$ $\mathbf{e}_2(s)$, and $\mathbf{e}_3(s)$ of $\Sigma(s)$ form a right-handed system
3. $\mathbf{e}_1(s)$ is the tangent to the backbone curve at $\mathbf{O}(s)$:

$$\mathbf{e}_1(s) = \mathbf{O}'(s)$$

4. $\mathbf{e}_1(0)$ and $\mathbf{e}_2(0)$ span the tangent plane $T_{\mathbf{O}(0)}(M)$ of the terrain surface at $\mathbf{O}(0)$ such that $\mathbf{e}_2(0)$ points to the right
5. $\mathbf{e}_3(0)$ is given as a binormal vector of $\mathbf{e}_1(0)$ and $\mathbf{e}_2(0)$ as $\mathbf{e}_3(s) = \mathbf{e}_1(s) \times \mathbf{e}_2(s)$ ($\times$ is the cross product)

6. according to Assumption 1.4, $\Sigma(s)$ does not twist around the backbone curve:

$$\langle \mathbf{e}_2'(s), \mathbf{e}_3(s) \rangle = \langle \mathbf{e}_2(s), \mathbf{e}_3'(s) \rangle = 0 \qquad \langle \cdot, \cdot \rangle : \text{inner product}$$

7. The shape of the backbone curve is characterized by two curvatures $\kappa_2(s)$ and $\kappa_3(s)$:

$$\kappa_2(s) = \langle \mathbf{e}_1'(s), \mathbf{e}_2(s) \rangle, \quad \kappa_3(s) = \langle \mathbf{e}_1'(s), \mathbf{e}_3(s) \rangle \qquad s \in (0, L)$$

These variables can be represented by one vector:

$$\kappa(s) = -\kappa_3(s)\mathbf{e}_2(s) + \kappa_2(s)\mathbf{e}_3(s) \tag{1}$$

On each edge, the vector is defined as

$$\kappa(0) = \lim_{s \to +0} \kappa(s), \quad \kappa(L) = \lim_{s \to -L} \kappa(s)$$

Note that the vector $\kappa(s)$ is perpendicular to the normal vector in Frenet-Serret theory, and so is parallel to the binormal vector. These definitions were set for technical reasons to facilitate subsequent vector operations.

2.1 Kinematics

To describe motion, the following conditions are assumed from a kinematic perspective:

Assumption 2.

1. *Every part of the backbone curve is constrained on the surface of the terrain*
2. *There is no sideslip*
3. *There is no constraint on relative rotation from the terrain around the backbone curve (except the head)*

These assumptions play a significant role in the proposed framework. The first relates to the environment, such as the weight of the body itself, surrounding debris, or a high-viscosity fluid. The second is known as the basic principle of lateral undulation. Snakes in nature have a specialized belly capable of this action. Some sort of device is needed to impart this condition in an artificial mechanism, such as a passive wheel or knife-edge. These constraints can be simply described by

$$\langle \dot{\mathbf{O}}(s), \mathbf{e}_2(s) \rangle = \langle \dot{\mathbf{O}}(s), \mathbf{e}_3(s) \rangle = 0$$

The third conditions is required in order to maintain consistency with Assumption 1.4.

According to conditions 1 and 2 above, every part of the body traces exactly the same trajectory as the head. Furthermore, the progress speed v along the backbone curve is uniform over the entire length due to the non-stretchability condition. Therefore, the curvature at $\mathbf{O}(s)$ of the current time t is the same as that of after a certain time Δt at $v\Delta t$ behind point $\mathbf{O}(s + v\Delta t)$.

$$\kappa(s + v\Delta t, t + \Delta t) = \kappa(s, t)$$

This leads to commutativity between $\dot{\kappa}$ and κ', as given by

$$\dot{\kappa}(s,t) = -v\kappa'(s,t) \qquad s \in (0, L],\ \kappa'(L,t) = \lim_{s \to -L} \kappa'(s,t) \tag{2}$$

The snake-like locomotive mechanism achieves forward motion by changing its shape. It is natural to let the time derivative of curvature $\dot{\kappa}(s)$ act a control values for such a kinematic model. Under the current conditions, however, the control values cannot be given arbitrarily due to Assumption 1. If there exists at least one point $s_0 \in (0, L]$ such that $\kappa_i'(s_0) \neq 0$ ($i = 2$ or 3), the progress speed v is given by $\dot{\kappa}_i(s_0)$ as follows.

$$v = -\frac{\dot{\kappa}_i(s_0)}{\kappa_i'(s_0)} \qquad i = 2 \text{ or } 3, \tag{3}$$

Once v is fixed, at the other points, $\dot{\kappa}(s)$ ($s \neq s_0$) is determined uniquely by the corresponding $\kappa'(s)$ according to Eq. (2).

Remark 1. *If $\kappa'(s) \equiv 0$ for all $s \in (0, L]$, that is, if the shape is a straight line or circular arc, there is no means to control the progress speed v. These shapes are called singular postures. Motion must be carefully planned so as to avoid these shapes.*

As long as the shape is not a singular posture, v and $\dot{\kappa}(s)$ can be regarded as identical. Hereafter, v is taken as one of the control inputs.

At the head point, a similar kinematic equation to Eq. (2) holds:

$$\dot{\kappa}(0) = -v\kappa'(0) \qquad \kappa'(0) = \lim_{s \to +0} \kappa'(s)$$

Note that $\dot{\kappa}(0)$ cannot be freely chosen since $\dot{\kappa}(0) = 0$ whenever $v = 0$. Therefore, $\dot{\kappa}(0)$ is not feasible for the control input. Moreover, $\kappa_3'(0)$ must follow the curvature (denoted K_{terrain}) of the terrain surface along $-\mathbf{e}_1(0)$. Thus, only $\kappa_2'(0)$ can be used as an additional control input.

The kinematic description is completed when all 6 DOFs of motion of $\Sigma(s)$ for each $s \in [0, L]$ are specified. Let $\omega_i(s)$ ($i = 1, 2, 3$) be the angular velocity of $\Sigma(s)$ around $\mathbf{e}_i(s)$. At every

point, from the curve geometry, the angular velocity of a reference frame is proportional to the curvature $\kappa_2(s)$, $\kappa_3(s)$ and the progress speed v:

$$\omega_2(s) = \kappa_3(s)v, \quad \omega_3(s) = -\kappa_2(s)v$$

By the assumption of no torsion, $\omega_1(s)$ is uniform along the entire length of the body:

$$\omega_1(s) = \omega_1(0) \qquad s \in (0, L]$$

Here, $\omega_1(0)$ depends on the profile of the terrain, that is, the rate of rotation (denoted R_{terrain}) of the surface along $-\mathbf{e}_1(0)$:

$$\omega_1(0) = R_{\text{terrain}} v$$

The full motion can then be summarized as follows.

Control input:

$$v = u_1, \qquad \kappa_2'(0) = u_2 \tag{4}$$

Shape:

$$\begin{aligned} \dot{\kappa}_2(0) &= -u_2 u_1 \\ \dot{\kappa}_3(0) &= -K_{\text{terrain}} u_1 \end{aligned} \tag{5}$$

$$\begin{aligned} \dot{\kappa}_2(s) &= -\kappa_2'(s) u_1 \\ \dot{\kappa}_3(s) &= -\kappa_3'(s) u_1 \end{aligned} \quad (s \in (0, L]) \tag{6}$$

Translation:

$$\langle \dot{\mathbf{O}}(s), \mathbf{e}_1(s) \rangle = -u_1, \quad \langle \dot{\mathbf{O}}(s), \mathbf{e}_2(s) \rangle = \langle \dot{\mathbf{O}}(s), \mathbf{e}_3(s) \rangle = 0 \tag{7}$$

Rotation:

$$\begin{bmatrix} \omega_1(s) \\ \omega_2(s) \\ \omega_3(s) \end{bmatrix} = \begin{bmatrix} R_{\text{terrain}} \\ \kappa_3(s) \\ -\kappa_2(s) \end{bmatrix} u_1 \qquad s \in [0, L] \tag{8}$$

2.2 Dynamics

Notions of mass, force and bending moment are introduced as listed in Table 1. The following assumptions are made to assist discussion of these dynamics:

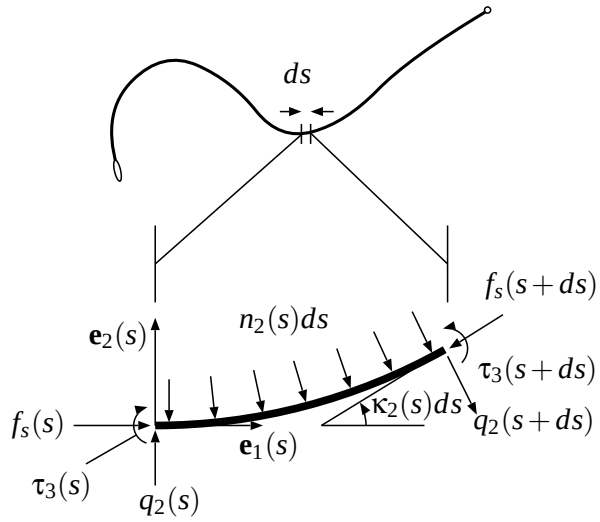

Figure 2. Forces acting on an infinitesimal slice of the backbone curve

Assumption 3.

1. *The bending moment can be generated on an arbitrary point except the edges*
2. *The moment of inertia of an infinitesimal piece around each axis is zero*
3. *The friction along the backbone curve is zero*
4. *Gravity does not affect the motion*
5. *The velocity is sufficiently small that the inertial force caused by velocity can be ignored*

Table 1. List of parameters for the dynamic model

ρ	Linear density of backbone curve
$f_s(s)$	Stress force along $\mathbf{e}_1(s)$
$n_i(s)ds$ $(i = 2,3)$	Distributed normal force along $\mathbf{e}_i(s)$
$q_i(s)$ $(i = 2,3)$	Shearing force along $\mathbf{e}_i(s)$
$\tau_i(s)$ $(i = 2,3)$	Bending moment around $\mathbf{e}_i(s)$

Recall that it is only necessary to deal with the 2 DOFs corresponding to u_1 and u_2 in Eq. (4). The parameter u_2 can be regarded as a sort of "steering" that only influences a small neighborhood near the head. The longitudinal motion is therefore discussed here. Figure 2 shows a slice of the backbone curve cut from the infinitesimal interval $[s, s+ds]$ projected onto the $\mathbf{e}_1\mathbf{e}_2$-plane with the relevant applied forces. The slice has curvature $\kappa_2(s)$ on this plane. Suppose that this slice is moving forward

with longitudinal acceleration $\alpha := \dot{u}_1$. The following three equations then hold from force balances:

Tangential balance:

$$\rho ds\alpha = f_s(s+ds)\cos(\kappa_2(s)ds) - f_s(s) - q_2(s)\sin(\kappa_2(s)ds) \tag{9}$$

Lateral balance:

$$n_2(s)ds = -q_2(s+ds)\cos(\kappa_2(s)ds) + q_2(s) - f_s(s+ds)\sin(\kappa_2(s)ds) \tag{10}$$

Momental balance:

$$\tau_3(s+ds) - \tau_3(s) + q(s+ds)ds = 0 \tag{11}$$

By taking the limit as $ds \to 0$, these three equations become

$$f_s'(s) = \rho\alpha - q_2(s)\kappa_2(s) \tag{12}$$
$$n_2(s) = -q_2'(s) - \kappa_2(s) f_s(s) \tag{13}$$
$$q_2(s) = -\tau_3'(s) \tag{14}$$

Substituting $q_2(s)$ in Eq. (12) with Eq. (14) and integrating Eq. (12) from 0 to s gives

$$f_s(s) = \rho s\alpha - \int_0^s \tau_3'(\sigma)\kappa_2(\sigma)ds$$

Since there is no stress at either edge, the boundary condition is given by

$$f_s(0) = f_s(L) = 0$$

Applying the formula of integration by parts yields

$$m\alpha = -\int_0^L \tau_3(s)\kappa_2'(s)ds \tag{15}$$

where $m := \rho L$ is the total mass.

A similar argument holds on the $\mathbf{e}_1(s)\mathbf{e}_3(s)$-plane with $\mathbf{n}_3(s)ds$ (distributed normal force along $\mathbf{e}_3(s)$), $q_3(s)$ (shearing force along $\mathbf{e}_3(s)$), and $\tau_2(s)$ (bending moment around $\mathbf{e}_2(s)$). The resultant equation is given by

$$m\alpha = \int_0^L \tau_2(s)\kappa_3'(s)ds \tag{16}$$

By the principle of superposition, Eqs. (15) and (16) can be integrated into one equation as follows.

$$m\alpha = -\int_0^L \left(\tau_3(s)\kappa_2'(s) - \tau_2(s)\kappa_3'(s)\right) ds$$

The right-hand side can be simplified using a vector:

$$\tau(s) = \tau_2(s)\mathbf{e}_2(s) + \tau_3(s)\mathbf{e}_3(s)$$

Using $\kappa(s)$ defined in Eq. (1), this leads to

$$\tau_3(s)\kappa_2'(s) - \tau_2(s)\kappa_3'(s) = \langle \kappa'(s), \tau(s) \rangle$$

Thus, the equation of motion along the backbone curve governing the entire motion is obtained as follows.

Equation of motion

$$m\alpha = -\int_0^L \langle \tau(s), \kappa'(s) \rangle ds \tag{17}$$

Remark 2. *It is clear from Eq. (17) that a singular posture in the kinematic model is also a singular posture in the dynamics model. In fact, if $\kappa'(s) = 0$ for all $s \in [0, L]$, the longitudinal acceleration is* 0.

2.3 Optimal Bending Moment

An infinite number of variations of the bending moment distribution are available. Here, an optimization problem involving minimization of the cost function of τ is adopted. Consider the cost function

$$J = \int_0^L \langle \tau(s), \tau(s) \rangle ds$$

and state the following problem:

Problem 1. *For a given α in Eq. (17), find the optimal bending moment distribution $\tau^*(s)$ that minimizes J.*

This problem is a sort of isoperimetric problem. According to the Lagrange multiplier method, a new functional x can be constructed as follows.

$$x = \int_0^L F_x(s)ds, \quad F_x(s) = \kappa'(s)\tau - \lambda\tau^2$$

The corresponding Euler equation is then

$$\frac{\partial F_x}{\partial \tau} - \frac{d}{ds}\frac{\partial F_x}{\partial \tau'} = \kappa'(s) - 2\lambda\tau = 0 \tag{18}$$

Solving this equation about τ and substituting the result into Eq. (17) leads to the following definition of the Lagrange multiplier λ:

$$\lambda = \frac{\int_0^L \langle \kappa'(s), \kappa'(s) \rangle ds}{2m\alpha}$$

This treatment gives the solution for the optimal bending moment:

Optimal bending moment

$$\tau^*(s) = -\frac{m\alpha}{\int_0^L \langle \kappa'(s), \kappa'(s) \rangle ds} \kappa'(s) \tag{19}$$

This equation reveals two features:

1. The distribution of optimal bending moment is similar to that of $\kappa'(s)$
2. Larger $\kappa'(s)$ allows the bending moment $\tau(s)$ to be smaller

The first property is quite convenient in the treatment of an articulated robot, as $\kappa'(s)$ can be easily approximated as the difference of joint angles.

3 Development of a Snake-like Robot

A prototype articulated robot with 9 links and 8 joints has been developed on the basis of this locomotive model, as shown in Fig. 3. Each joint has a universal joint-like structure with 2 DOFs, allowing the body to bend in two ways (Fig. 4). All joints are actuated by direct-current (DC) motors. Each link is equipped with a control board and passive wheels. The control boards consist of a one-chip microcomputer and 2 pairs of field effect transistor (FET) H-bridge motor drivers, and each board is connected to the adjacent board via a serial connection. A summary of the specifications of the prototype is provided in Table 2. The passive wheels generate constant force against sideslip, as required by Assumption 2.2. The axle of the passive wheel can freely rotate around the body axis (except for the head link), satisfying Assumption 2.3 (Fig. 5). As the model requires torque-based control, joint flexibility is an important capability. To this end, a small motor and gearing system with low friction and backlash is employed.

The kinematic parameters in the continuum model can be translated into the articulated model as shown in Table 3. Note

Figure 3. Overview of 9-link locomotive mechanism

Table 2. Specification of prototype

Total mass	2.8 [kg]
Total length	0.9 [m]
Microcomputer	Renesas H8/3664 × 9
DC motor	Maxon Re-max 17 × 17
Power source	Ni-MH 2000 mAh × 6

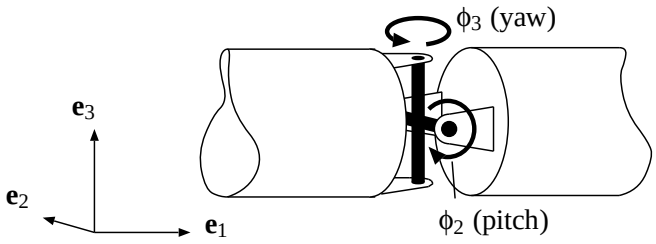

Figure 4. Joint structure

that $\kappa_2(s)$ corresponds to ϕ_3^i, and $\kappa_3(s)$ to $-\phi_2^i$. The optimal bending moment (Eq. (19)) can then be discretized to give the following approximation:

$$\begin{bmatrix} \tau_2^*[i] \\ \tau_3^*[i] \end{bmatrix} = -\frac{m\alpha n^2}{L^2 \sum_{i=2}^n (\Delta\phi_2[i]^2 + \Delta\phi_3[i]^2)} \begin{bmatrix} \Delta\phi_2[i] \\ \Delta\phi_3[i] \end{bmatrix} \tag{20}$$

where $\Delta\phi_k[i] = \phi_k[i] - \phi_k[i-1]$ $(k = 2,3)$. The tasks of the ith controller are summarized as follows.

1. Receive the joint angles $\phi[i-1] := (\phi_2[i-1], \phi_3[i-1])$ from the previous link

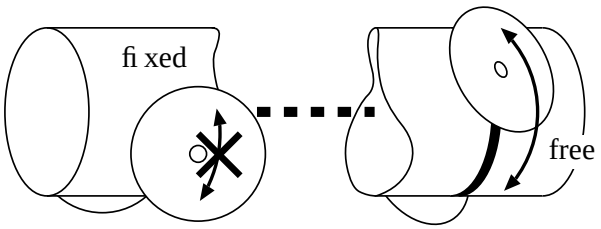

Figure 5. Axle of passive wheel

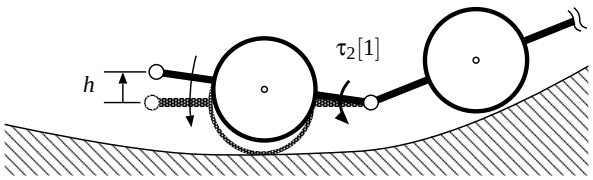

Figure 7. Lifting/bowing control of the head link

Table 3. Parameters in continuum model vs. articulated model

Continuum model		Articulated model	
Arclength	$s \in [0, L]$	$i = 1, \cdots, n-1$	Joint number
Curvature	$\kappa_2(s), \kappa_3(s)$	$\phi_2[i], \phi_3[i]$	Joint angle
Bending moment	$\tau_2(s), \tau_3(s)$	$\tau_2[i], \tau_3[i]$	Joint torque

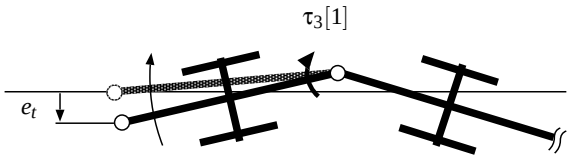

Figure 8. Tracking control to desired path

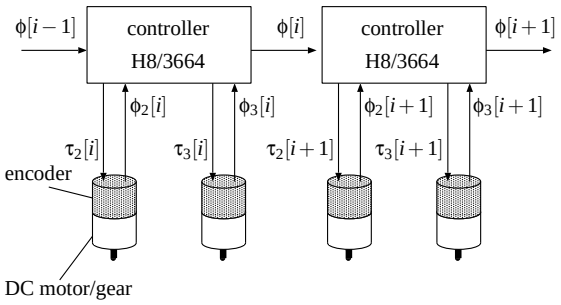

Figure 6. Schematic of control system

2. Calculate and apply the desired joint torque $\tau_2[i]$ and $\tau_3[i]$ according to Eq. (20)
3. Transmit the joint angles $\phi[i] := (\phi_2[i-1], \phi_3[i])$ to the succeeding link

A schematic of the controller is shown in Fig. 6.

4 Locomotion on smooth 3D surface

In order to explore a smooth 3D surface, the head link must follow the terrain surface, requiring special control for the first joint. Figure 7 describes a situation in which the head link "floats" up from the terrain surface. In this case, $\tau_2[1]$ is used for the bowing action in recovering contact with the surface, as follows.

$$\tau_2[1] = -K_2 h - D_2 \dot{\phi}_2[1]$$

where h is the error from the desired distance from the surface measured by a distance sensor, K_2 is the coefficient of stiffness, and D_2 is a damping coefficient. In this case, $\tau_3[1]$ is a kind of steering torque, similar to that of a car model, and is used for reducing tracking error from the desired trajectory (Fig. 8). Tracking error e_t is measured by a tracking arm (Fig. 9). Many conventional methods for line tracing robots can be applied in this way. In the present case, the following control law is applied:

$$\tau_3[1] = -K_3 e_t - D_3 \dot{\phi}_3[1]$$

For other links, the joint torques are given by Eq. (20) and are approximately optimal in the sense of mechanical stress on the actuator. Although Eq. (20) includes information on all joints, the desired progress speed v_d can be obtained as follows without using this information.

$$\begin{bmatrix} \tau_2[i] \\ \tau_3[i] \end{bmatrix} = -K(v_d - v) \begin{bmatrix} \Delta\phi_2[i] \\ \Delta\phi_3[i] \end{bmatrix} \tag{21}$$

where K is a constant feedback gain. This is equivalent to setting

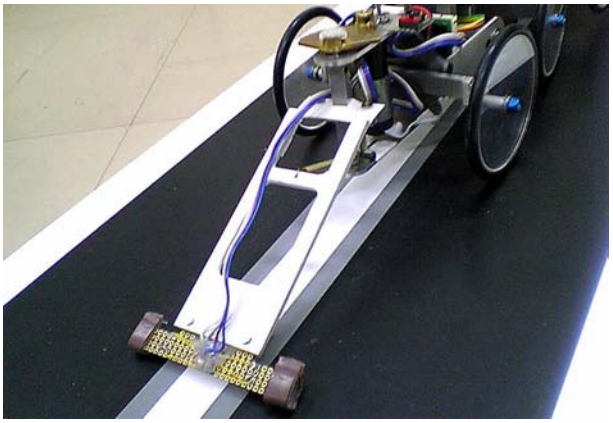

Figure 9. Tracking arm

the acceleration α by

$$\alpha = \dot{v} = K(v_d - v)\frac{L^2 \sum_{i=2}^{n} (\Delta\phi_2[i]^2 + \Delta\phi_3[i]^2)}{mn^2} \qquad (22)$$

It is clear that v converges to v_d as long as the posture is non-singular and there is no disturbance. Thus, the set of data that should be transferred between links via serial communication consists of $\phi_2[i]$, $\phi_3[i]$, v, and v_d. It should be emphasized that the order of complexity is just $O(1)$, and is independent of the number of links.

4.1 Simulation

Computer simulations were performed to verify whether the proposed control strategy will work for exploration over unknown 3D terrain. The simulation model was constructed using Autolev^{TM} (Online Dynamics Inc.), a symbolic manipulation software package. The contact conditions were modeled as a spring-damper system, and the physical parameters were chosen such that the behavior was as close to the real system as possible. The prescribed task was traversal over a small ridge. Figure 10 shows snapshots of the resultant animations created by Scherzo (free software using OpenGL). The robot is initially placed in a flat area and formed into a winding shape to avoid a singular posture at the outset. The robot moves toward the left. When it arrives at the ascent, it raises its head and follows the surface. The uphill part of the body is thrust by the succeeding links on the flat area until it reaches the crest, beyond which traction is re-established and is transmitted to the succeeding link (3rd figure). At this time, the robot can progress without a horizontal winding gait. It is important that non-floating condition, Assumption 2.1, are satisfied.

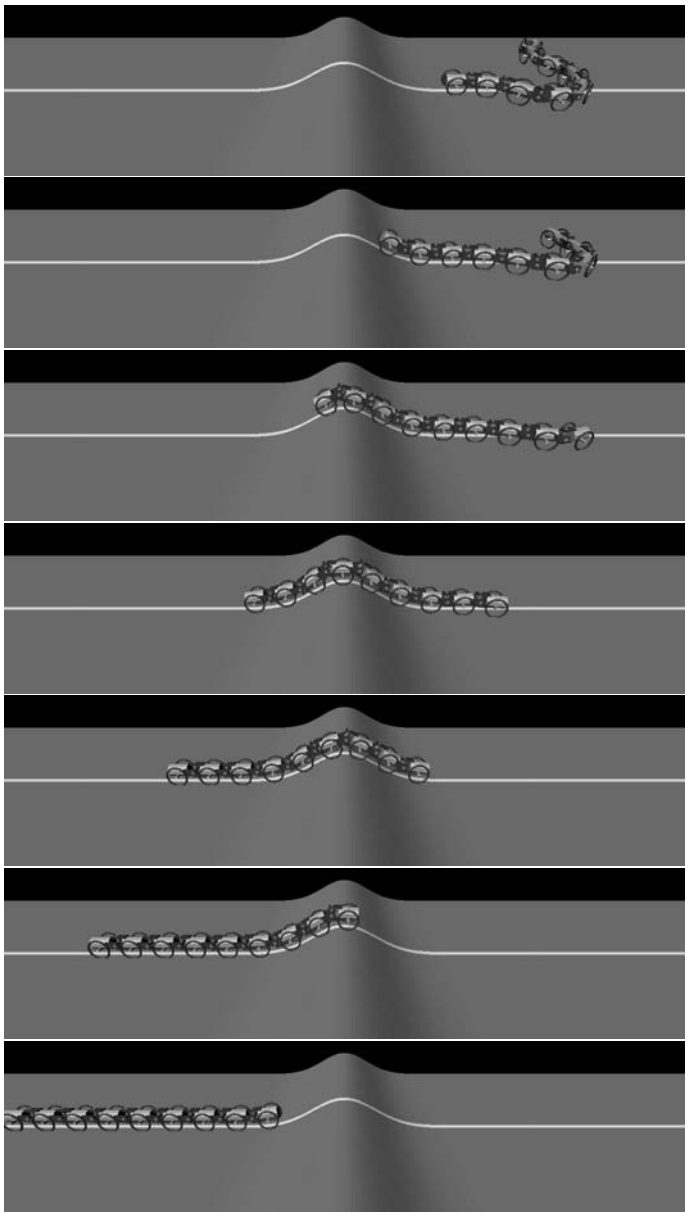

Figure 10. Snapshots of simulation

4.2 Experiment

A corresponding experiment was performed using the prototype. As a suitable distance sensor could not be obtained for surface following in this experiment, the initial position was set as shown in Fig. 11. A total of 5 retro-reflective markers were attached to the top of the head, 2nd, 4th, 6th, and 8th joints for observation using a motion capture system (Qualisys Inc.). Figure 12 shows the loci of these points in the *xz*-plane (plumb plane). Each point draws an almost identical trajectory without floating from the surface.

Figure 11. Experiment

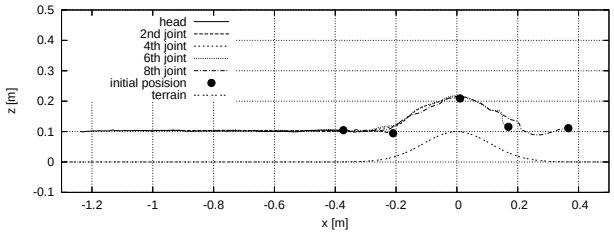

Figure 12. Loci of markers in *xz*-plane

5 Conclusion

A continuum model for snake-like creeping locomotion over a smooth 3D surface was proposed. The kinematics and dynamics of the system were derived using simplified assumptions, and a control law for locomotion over unknown 3D terrain was proposed. The optimal bending moment is found to have quite a simple form. Despite the simplifications, however, the proposed method was demonstrated to be effective for traversing unknown 3D terrain through both simulation and experiments using a prototype robot. A bcontrol algorithm and mechanism for non-smooth terrain are logical extensions to this model that should be addressed in future work.

REFERENCES

[1] Hirose, S., 1993. *Biologically Inspired Robots*. Oxford University Press.

[2] Ostrowski, J., and Burdick, J., 1996. "Gait kinematics for a serpentine robot". In Proc. of the IEEE International Conference on Robotics and Automation, pp. 1294–1299.

[3] P.Prautsch, and T.Mita, 1999. "Control and analysis of the gait of snake robots". In Proc. of the IEEE International Conference on Control Applications, pp. 502–507.

[4] Date, H., Hoshi, Y., and Sampei, M., 2000. "Locomotion control of a snake-like robot based on dynamic manipulability". In Proc. of the IEEE/RSJ International Conference on Intelligent Robots and Systems, pp. 2236–2241.

[5] Ma, S., Ohmameuda, Y., Inoue, K., and Li, B., 2003. "Control of a 3-dimensional snake-like robot". In Proc. of the IEEE International Conference on Robotics and Automation, pp. 2067–2072.

[6] Chirikjian, G., and Burdick, J., 1995. "The kinematics of hyper-redundant robot locomotion". *IEEE Transactions on Robotics and Automation*, **11**(6), pp. 781–793.

[7] Chirikjian, G., and Burdick, J., 1995. "Kinematically optimal hyper-redundant manipulator configurations". *IEEE Transactions on Robotics and Automation*, **11**(6), pp. 794–806.

[8] Ghirikjian, G., 1995. "Hyper-redundant manipulator dynamics: a continuum approximation". *Advanced Robotics*, **9**(3), pp. 217–243.